https://ntrs.nasa.gov/search.jsp?R=19690026877 2020-03-12T05:16:45+00:00Z

N69-36255
CR-86224

C5-1471.11/3111 Copy 87

PROCESS TECHNIQUES STUDY OF INTEGRATED CIRCUITS

Quarterly Report No. 11

February 15, 1968

Prepared by:

J. E. Meinhard

AUTONETICS
A DIVISION OF NORTH AMERICAN ROCKWELL CORPORATION
3370 Miraloma Avenue, Anaheim, California 92803

Prepared Under Contract NAS 12-4
General Order 06433

APPROVED BY:

P. H. Eisenberg
Group Scientist
Materials Reliability
Physical Sciences

APPROVED BY:

H. C. Mattraw
Acting Manager
Materials Technology
Physical Sciences

158-D-3 REV. 9/67

PROCESS TECHNIQUES STUDY OF INTEGRATED CIRCUITS

Quarterly Report No. 11

ABSTRACT

The purpose of this program is to investigate some of the dominant problems confronting planar technology, to seek solutions to these problems and to provide instrumental support services to NASA-ERC in the areas of failure analysis and instrumental capabilities. Areas of investigation are organized under the following four categories of activity.

Investigational Activities:

1. Failure Mechanisms Related to Oxide Passivation
2. Failure Mechanisms Associated with Packaging

Services:

1. Failure Analysis Service and Consultation
2. Instrumental Capability Profile

Past program activities on oxide passivation have provided insights into the origin of atomic species contributing to inversion and the origin of dielectric defects. Current activities are concentrated primarily on the latter problem where it has been shown that most of the dielectric defects in oxide layers are developed during the cooling of wafers after oxidation and follow an exponential decay with increasing oxide thickness. Present experiments show that diffusion barriers introduced prior to oxidation tend to reduce virtual defect densities and lead to a lateral ion migration model to account for initial inhomogeneous oxide distribution.

Previous packaging investigations have been confined to gas ambient studies in which the effects of hydrogen and of water were evaluated on the performance of various transistor samples. The program has been extended to other failure problems of importance to packaging as well as to environmental studies on integrated circuits. The present report summarizes investigations which show the effects of hydrogen on integrated circuits to be nonspecific and innocuous. A listing of interactions involving potential package components also has been compiled giving thermodynamic free energy values and kinetic data of possible utility in the prediction of long term device stability.

Failure analysis on Case Number CQF-101, comprising 89 npn transistors has been completed.

The instrumental capability profile provided at an early stage of this program has been updated in the present report.

PROCESS TECHNIQUES STUDY OF INTEGRATED CIRCUITS

Quarterly Report No. 11

1. Failure Mechanisms Related to Oxide Passivation

The occurrence of dielectric defects, or "pinholes", constitutes a significant failure mode in modern oxide passivated devices and is probably the largest remaining barrier to large scale integration. Although numerous remedial innovations in materials and process techniques have been attempted, no reliable solution to this problem has yet been found. Because of the general convenience and superiority of thermally grown oxide for most masking and passivating purposes, and because this application of silicon dioxide has been successfully optimized in most other respects, it seems important to take full advantage of these characteristics by determining the process requirements needed to remove this remaining major problem in its use. The objectives of this effort, therefore, are to discover why structural defects are produced in thermally grown oxides and to learn how they may be prevented.

Previous activity on this program has sought to relate the origin of dielectric defects to various process factors and structural considerations. These results may be summarized as follows:

A. Factors tending to increase dielectric defects.

- a. Extended processing (generally).
- b. Higher compressive stress in the oxide.
- c. Embedded lapping grains in the substrate.
- d. Superficial HF etching.
- e. Abrupt oxide steps.
- f. Thermal cycling.
- g. Mechanical wiping.
- h. Removal of back oxide layers.

B. Factors tending to decrease dielectric defects.

- a. Growth of oxide to higher thicknesses.
- b. Chemical etch of initial wafer.
- c. Pyrolytic oxide, uniformly applied and properly densified.
- d. Additives tending to reduce bond strain in silica glass.
- e. Addition of steam to oxidation process gas, or termination of any dry oxidation step with a wet oxidation.

C. Factors having little or no effect on defect incidence.
   a. Wafer cooling rates after oxidation.
   b. Mineral content of water used as steam source.
   c. Oxide growth rate.
   d. Substrate doping (generally).
   e. Crystal defects (dislocations and stacking faults).
   f. Certain non-reactive particulate contaminants (such as alumina) which do not stick to the oxide during growth.

Electron photomicrographs show pile-ups of oxide layers at defect sites, thereby indicating compressive stress in the oxide as the major cause of defects. This idea was confirmed by comparing oxide defect densities existing at the oxidation temperature with those existing after cooling. Briefly, the technique consists of terminating an oxidation with a short HCl etch which attacks any exposed silicon, producing an etch pit at each defect site. After cooling the additional defects are located by electrophoretic decoration. In an oxide layer grown to 8000Å the ratio of defect densities before and after cooling was found to be 1:195. Most of the above findings have been reported previously[1,2] and all are consistent with the compressive stress model advanced as the originating agency of oxide defects.

The approaches to continued investigation on this program consist of examining in detail the inhomogeneities in oxide distribution evidently present at the initial stages of oxidation using the techniques described above. Experiments have shown that a significant number of defects may exist at the processing temperature after only a brief oxidation period, thus predisposing oxides to a distribution of thin spots at later stages of oxidation. It is postulated that a portion of these thin spots yield to the compressive stress produced on cooling and that the remainder constitute the latent defect sites opened up by light etching in hydrofluoric acid. It is further postulated that if initial oxidation irregularities could be removed through appropriate process control the finished oxide layers would be free of thin spots and capable of withstanding the existing stresses without rupture.

More quantitative investigations were conducted to compare defect densities at no stress (i.e., before cooling), at full stress (i.e., after cooling) and at partial stress relief (i.e., after removal of the back oxide layer). These data were obtained for a series of oxidation times in order to yield growth dependent plots as typified in Figures 1 and 2. Conventional oxide growth technique was used (N_2: 245 cc/min; O_2: 245 cc/min passed through water at slightly less than 100C; temperature: 1180 C) followed by HCl-He etching before removal from the growth zone. Defect densities were evaluated by standard etch pit and decoration counts. The observed dependence on $t^{\frac{1}{2}}$ is characteristic of a diffusion controlled process and has been confirmed by other investigators[3-9] for the oxidative growth of silica. The exponential decrease in the number of defects with oxide growth also is apparent from Figures 1 and 2. Decay of this number, N, may be expressed either in terms of growth time, t, or layer thickness, Z, according to

$$N = N_t e^{-\lambda t^{\frac{1}{2}}} = N_z e^{-\phi z} \quad (1)$$

where N_t and N_z are the corresponding preexponential factors (ordinate intercepts) and λ and ϕ are the respective decay factors. Decay factors appropriate to Figures 1 and 2 are listed in Table I:

TABLE I. OXIDE DEFECT DECAY FACTORS

Condition	λ (minutes$^{-\frac{1}{2}}$)	ϕ (per 1000Å)	λ/ϕ
No stress	1.37	2.22	.62
Full stress	0.60	1.08	.55
Partial stress	0.45	0.83	.54

Internal consistency between the time and thickness data is given by the ratios, λ/ϕ , and is better than 94 percent.

Obviously the smaller the decay factor the greater the defect density and the more serious the pinhole problem. Merely by cooling from the oxidation temperature to room temperature the decay factor is reduced by more than 50 percent and the defect density increased by roughly an order

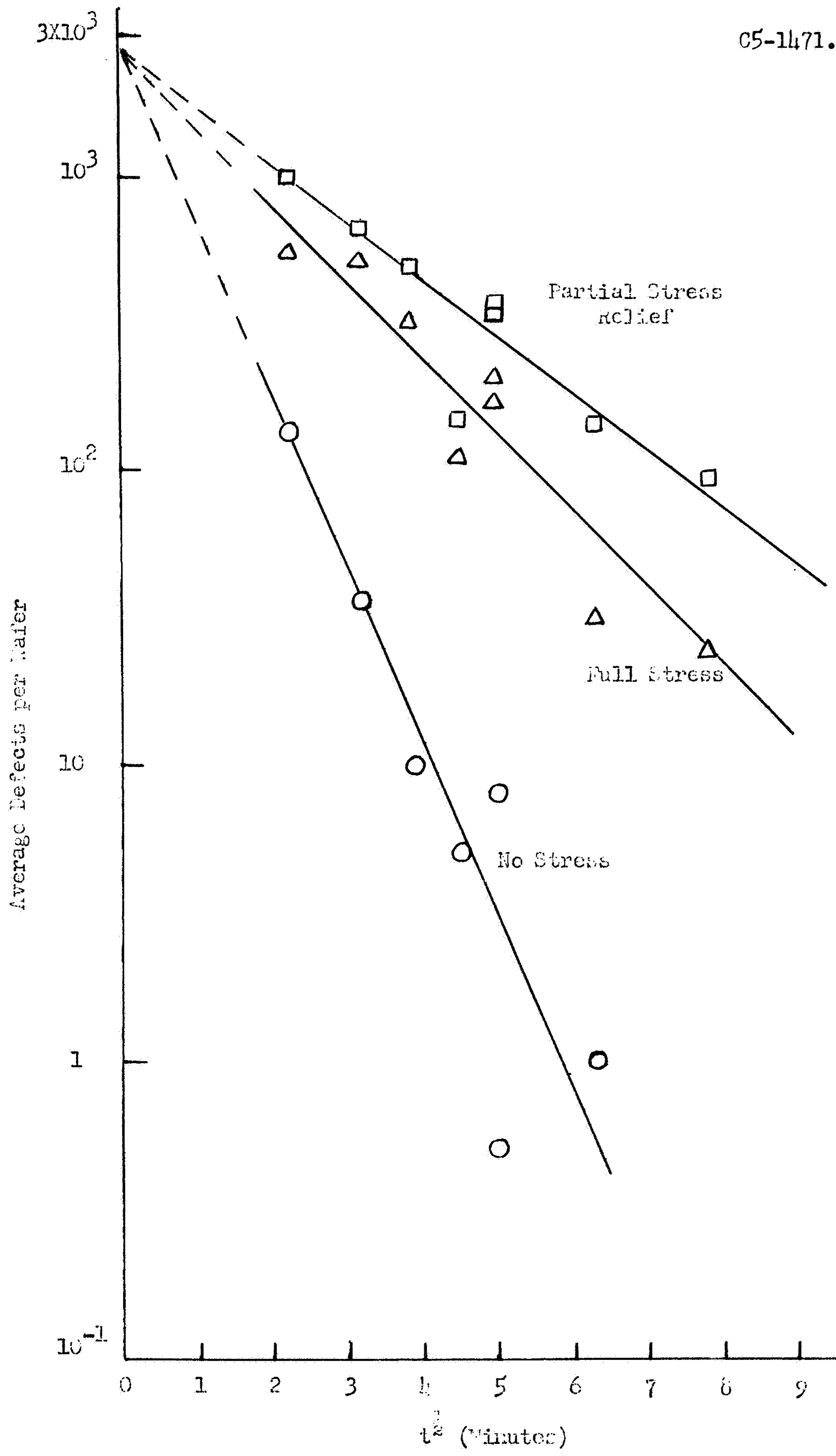

Figure 1. Defects as a Function of Oxidation Time for Various Stress Conditions.

C5-1471.11/3111

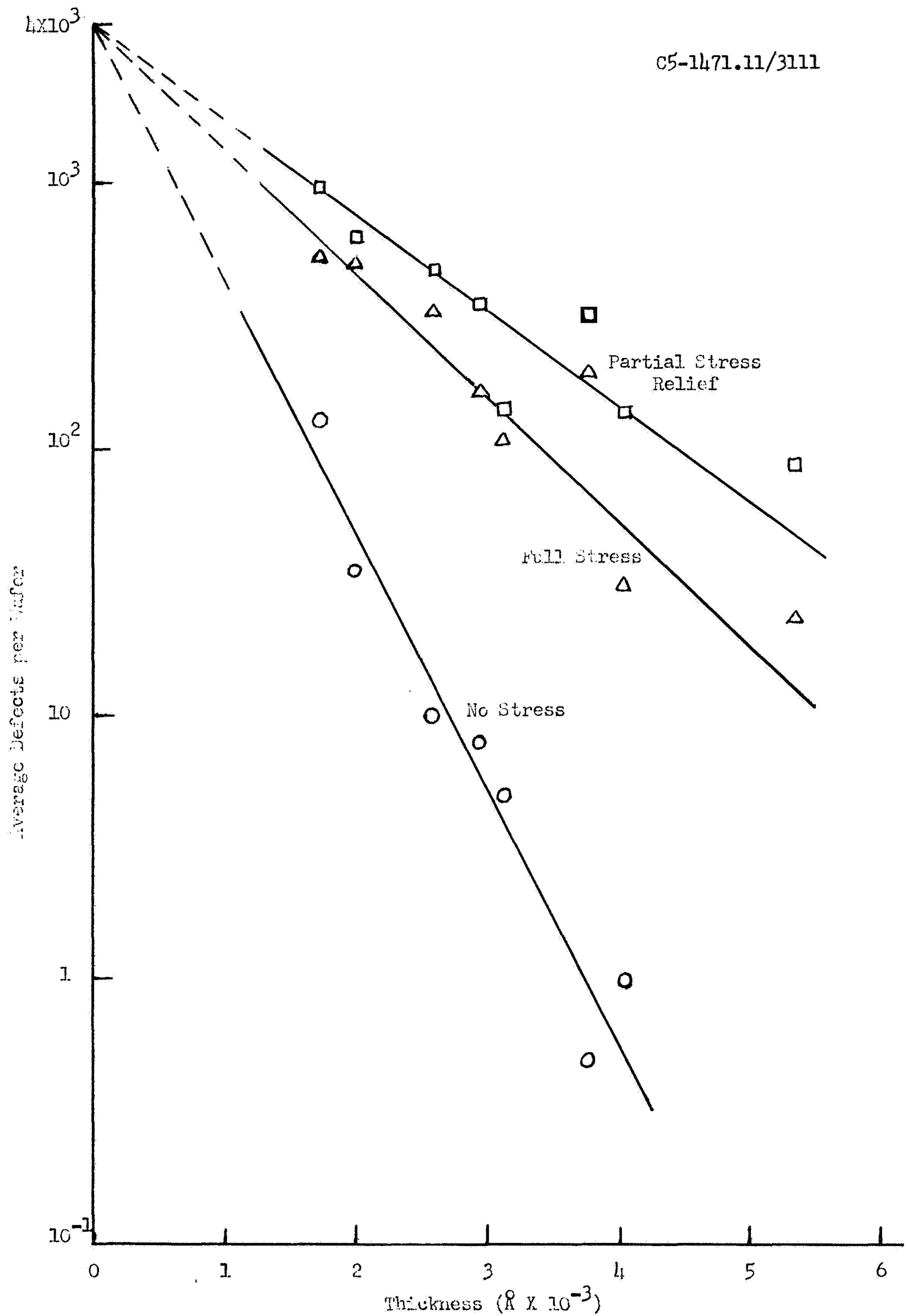

Figure 2. Defects as a Function of Oxide Thickness for various Stress Conditions.

of magnitude. Simultaneously with cooling the compressive stress is developed in the oxide layers which, for the set of wafers under discussion, was found by Proficorder analysis to be uniformly 4.1×10^{-4} psi[10] over the range of thicknesses grown (see Appendix A). It is this magnitude of stress that differentiates the "full stress" condition (middle curve) from the "no stress" condition (lower curve) existing at the oxidation temperature. And it is the difference in slopes of these two curves that links the occurrence of dielectric defects with compressive stress.

In the upper curve stress in the oxide layer has been partially relieved by etching off the opposite oxide layer. The relief mechanism is through strain of the silicon substrate, yielding an observable warp curvature in the wafer. As a result the remaining oxide layer assumes a conformal convex curvature which, it is postulated, opens up oxide fracture sites previously held together in the more planar "full stress" state. Thus, the "partial stress relief" condition is believed to introduce still more defects, as evidenced by the slope of the upper curve in Figures 1 and 2, because of the unbalanced nature of the relief. It would appear from these results that an integrated circuit technology that allowed the back oxide to remain on the chip would be somewhat less prone to pinhole problems.

A more serious problem, however, remains. This is the existence of a virtual defect density (N_t, equation 1) of the order of $10^3/cm^2$. Admitting that this extrapolated value is fictitious, one still must assume a very large defect density at some small $t > 0$ which increases exponentially with thinner oxides. This problem is especially critical to MOS-FET technology where gate oxides of 1000Å, or less, are generally required. It seems more important, therefore, to understand the physical basis for the virtual defect density, so that it can be manipulated downwards, rather than attempting to increase defect decay factors. Furthermore, on the assumption that oxide growth (and defect mending) must remain constitutionally invariant, there would appear to be very little opportunity at all for affecting decay factors one way or the other.

From a comparison of Figures 1 and 2 it is seen that the preexponential defect density is approximately 50 percent higher for the thickness dependent

curves than for the $t^{\frac{1}{2}}$ dependent curves. This difference is significant within the experimental limits of error and suggests that the reaction kinetics governing the initial phases of oxidation differ from those applicable to the remainder of the process. It appears reasonable that the time dependent curves would tend to become asymptotic in the vicinity of the ordinate, but no firm conclusion of this nature can be drawn on the present evidence. Of more practical significance is the evidence afforded by these plots of nonhomogeneous oxide distribution at the beginning of oxidation, and its possible association with the anomalous reaction kinetics in that phase of the process. If this is the case, process steps or modifications capable of moderating the initial oxidation kinetics should have a significant effect on the virtual, and hence ultimate, defect densities.

Initial efforts to test this hypothesis were directed toward wafer pretreatments designed to produce diffusion attenuation layers on the surfaces. These layers consist primarily of silicon dioxide in the 200Å or less thickness range produced by wet chemical methods and have shown initial encouraging results. Briefly the method consists of treating the wafers with HF (to remove old oxide), 50 percent KOH at 50C (to remove residual flouride), and hot concentrated nitric acid (to remove residual KOH and initiate uniform oxidation). Each step is followed by thorough rinsing with distilled water. Initial tests revealed zero defects under conditions of no stress after only 15 minutes of oxidation. Therefore shorter oxidation times were investigated which were expected, on the basis of previous results, to yield higher defect densities. Hydrogen chloride etch-pits in the silicon produced under no-stress conditions are listed in Table II.

TABLE II. INFLUENCE OF WAFER PRETREATMENT ON INITIAL OXIDE DEFECTS

Sample	Oxidation Time (minutes)	Volume HCl in He (%)	Etch Pits (average per wafer)
1	2.5	3.5	0.5
2	5	3.5	0.5
3	5	2.6	1.0
4	5	3.0	3.0
5	10	3.4	1.0
6	15	3.0	4.0
7	15	3.9	0.0

These results appear to indicate that the pretreatment exerts substantial control over the incidence of initial defects to the extent that the previously found exponential dependence on growth time is absent and no significant extrapolation to latent defect density at zero time is possible. This effect represents a significant departure from previous results and requires further verification.

A second set of wafers, therefore, was pretreated with nitric acid as above and exposed to a sequence of increasing oxidation times without a terminal HCl vapor phase etch. On cooling to room temperature these wafers were examined by electrophoretic decoration, yielding the results listed in Table III and plotted in Figure 3.

TABLE III. FULL STRESS DEFECT DENSITIES IN PRETREATED WAFERS

Run	Oxidation Time (minutes)	Oxide Thickness (Angstroms)	Defects per wafer (Average)
K	2.5	1300	213±18
L	5	2000	172±29
M	10	2700	88±11
N	15	3000	75± 6
O	20	4100	50± 3
P	30	5000	40± 3

It is immediately apparent that the virtual (preexponential) defect densities are reduced by a factor of almost 10 by the wafer pretreatment. However, this is still substantially higher than expected on the basis of the etch count data in Table II. The underlying mechanism responsible for this effect of the nitric acid pretreatment is still unresolved.

It also can be seen from Figure 3 that the virtual defect density is now higher for the time dependent plot than for the thickness dependent plot---a reversal of the trend found for the untreated wafers. It appears, therefore, that the wafer pretreatment with nitric acid does in fact slow the initial oxidative attack. This becomes more apparent by plotting

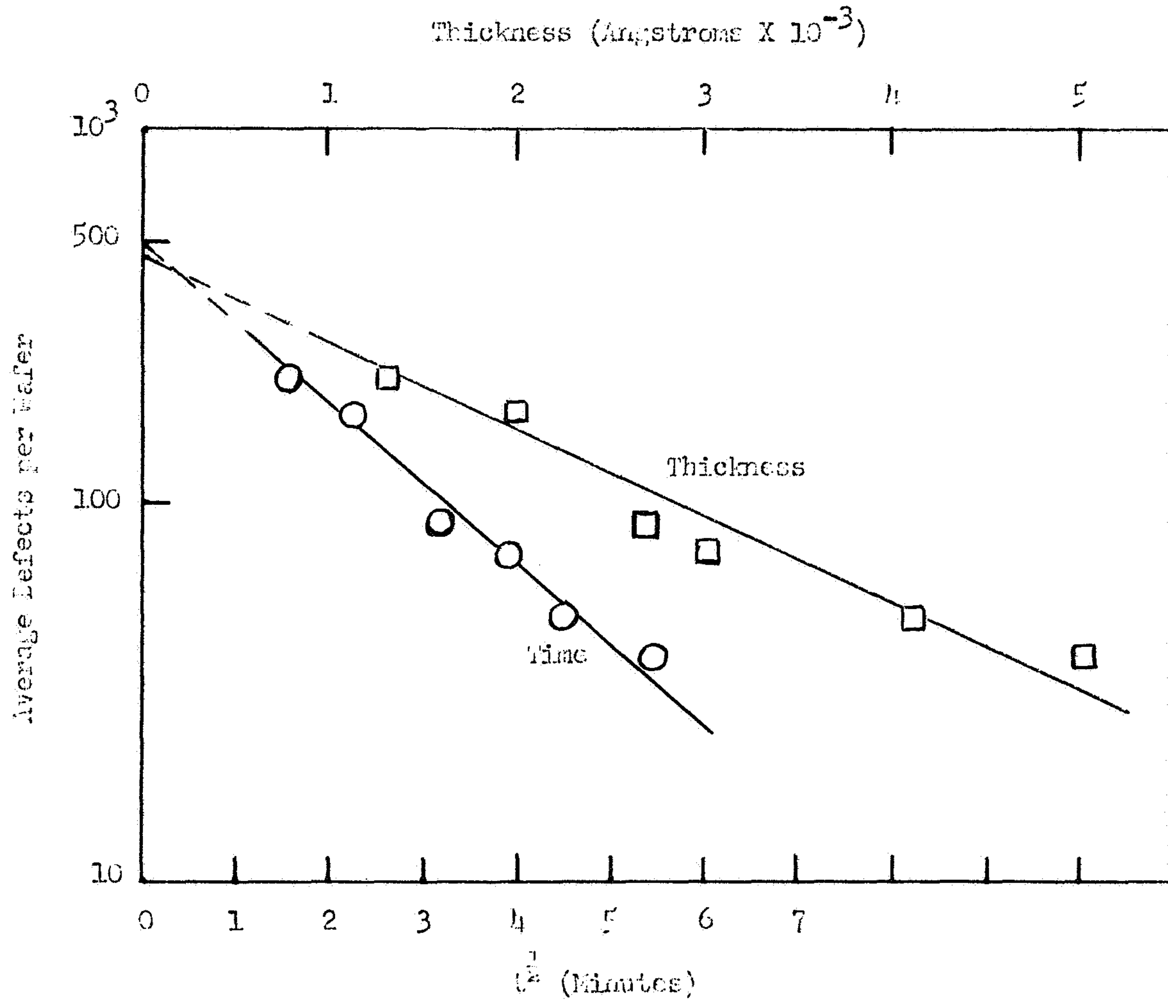

Figure 3. Oxide Defects as a Function of Growth for Pretreated Wafers.

thickness versus $(\text{time})^{\frac{1}{2}}$ for the two sets of wafers as shown in Figure 4. The "treated" curve is concave near the origin whereas the "untreated" curve is convex, again suggesting that the treatment initially attenuates oxygen diffusion to the silicon. The difference in slopes is due to an increase in water injection for the treated series.

The exact nature of the layers produced by the nitric acid still are unknown. Boundaries in such layers produced by controlled (masked) HF etching are readily revealed by moisture condensation from a humid environment. Attempts to measure the thickness of the layers by Proficorder and Tally-Surf tracing, and by interferometry, however, have failed. Although the layers are suspected of being a porous and partly hydrated silicon dioxide, the possibility of a small component of nitride cannot be ruled out.

Following the kinetic clues to the control of oxide defects developed above a series of wafers was pretreated with a slow-growth oxide layer (250Å in 0.5 hour, O_2:N_2 = 1:48) prior to normal oxide growth to varying thicknesses (2500-4300 Å). The results are plotted in Figure 5 and show essentially negligible improvement over those plotted in Figure 1. Since this pretreatment was made at normal growth temperature it can be assumed that the conditions leading to inhomogeneous oxide distribution in the initial phase of oxidation were essentially unchanged.

In summary it may be said that the very presence of a virtual defect density implies an inhomogeneous distribution of oxide at the start of oxidation which is progressively "mended" by continued oxidation. The mending process is observed to be random both in temporal and spatial distribution, resulting in a population of thin spots of varying degrees of thickness. The major question to be answered is what produces this initial inhomogeneity. The answer is being sought by the use of two types of experiment: extrapolation of oxidation kinetic data to time zero and examination of the effects of process variants on oxide morphology after extremely limited oxidation.

Process variants investigated thus far include a hot nitric acid pretreatment of wafers (previously reported[10]) and a slow initial growth

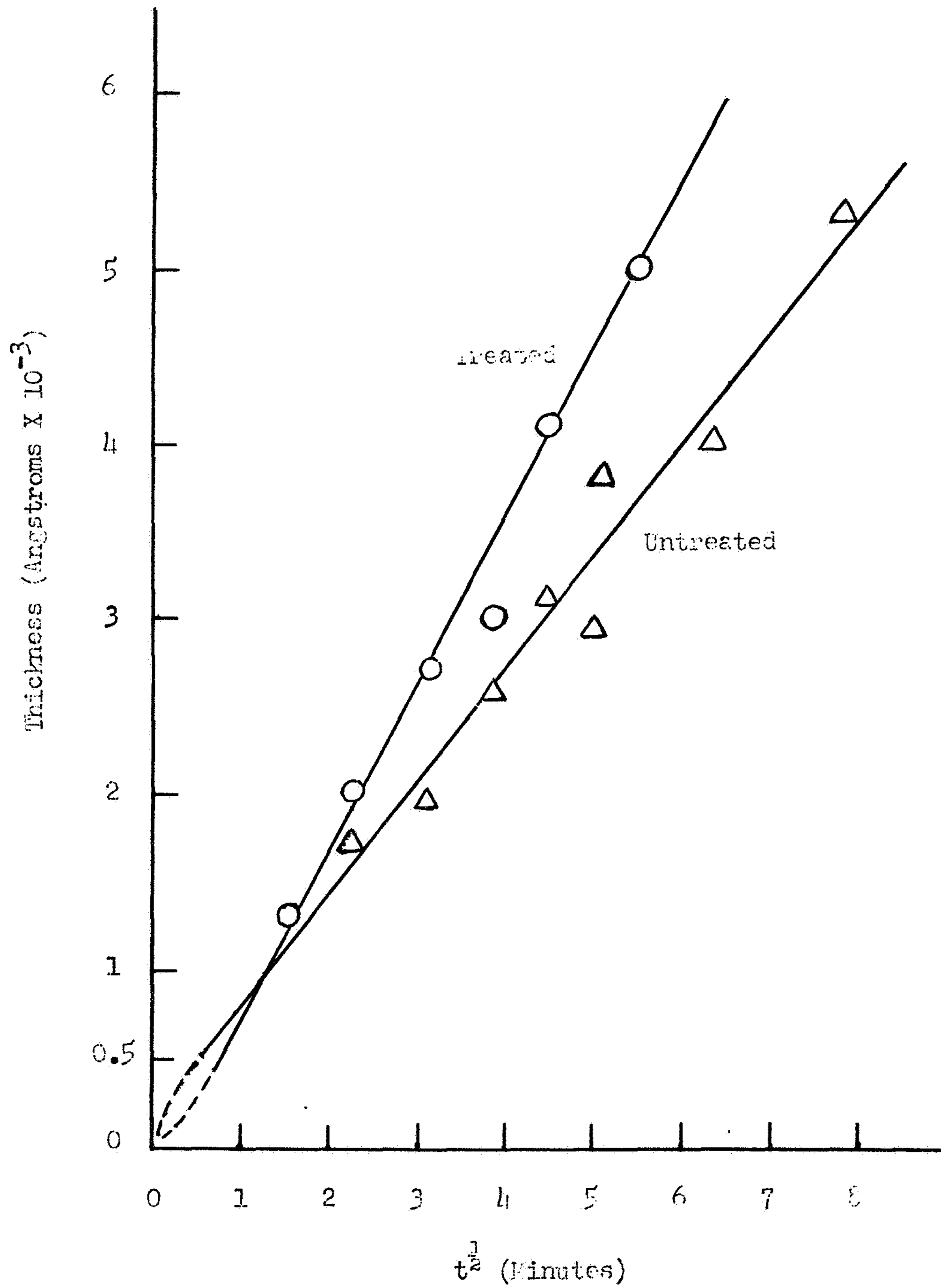

Figure 4. Oxide Thickness Dependence on Time for Treated and Untreated Wafers.

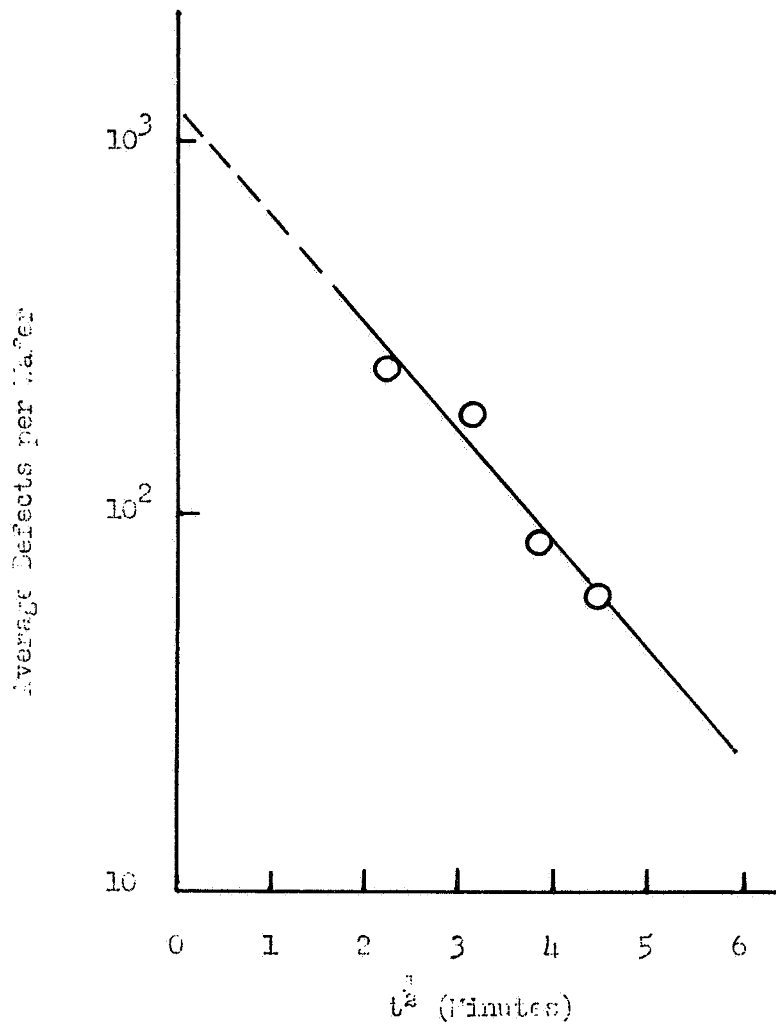

Figure 5. Defect Decay Preceded by Slow-growth Oxide.

of oxide achieved by limiting the oxygen concentration (to about 2 percent v/v) during the first half hour of oxidation. Initial results of these experiments indicate the following:

1. A kinetic anomaly exists during the first minute or two of oxidation which is in the direction of an accelerated rate (vs a strictly linear dependence on $t^{\frac{1}{2}}$) for wafers precleaned by normal technique and a decelerated rate for wafers pretreated with hot nitric acid.
2. Pretreatment of wafers with hot nitric acid appears to reduce the virtual defect density to a negligible value for the unstressed condition (i.e., before cooling), but the virtual defect density after cooling is lower only by a factor of about ten.
3. Pretreatment of wafers by slow initial oxide growth (about 250Å in the first half hour) at 1180 C produces essentially no reduction in virtual defect density for the full stress condition.

The latter two observations require further verification. If validated, however, they lead to the speculation that the initial rate of oxidation of silicon atoms is lower (i.e., more hindered) than at some subsequent but still incomplete oxidation state, SiO_x ($x < 2$). Assuming, at 1180 C, a lateral mobility of oxygen ions on a silicon surface, SiO_y ($y < x$), any SiO_x present will tend to usurp incoming oxygen via transport through SiO_y. One way to formulate the sequence of events is as follows:

$$SiO_x + SiO_y \rightarrow SiO_2 + Si \qquad (2)$$

$$Si + O_2 \rightarrow SiO_y \qquad (3)$$

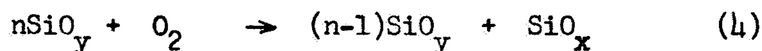

$$nSiO_y + O_2 \rightarrow (n-1)SiO_y + SiO_x \qquad (4)$$

The model requires, however, that each molecular "unit" of SiO_2 produced leave behind an adjacent SiO_x to continue the local propagation. The model predicts a distribution of latent oxide defects equivalent to the initial distribution of SiO_x, which is determined in turn by the surface mean free path of oxygen ion diffusion via SiO_y.

A more graphic representation of the model may be depicted as follows:

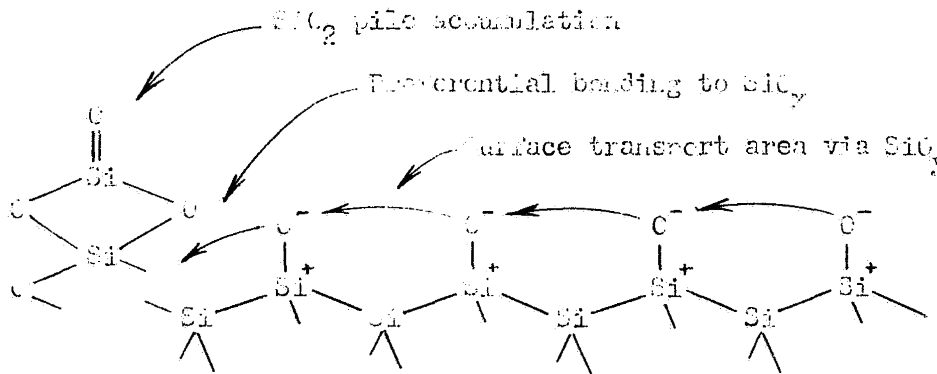

The localized oxide aggregates in the beginning stages of oxidation may be visualized as follows:

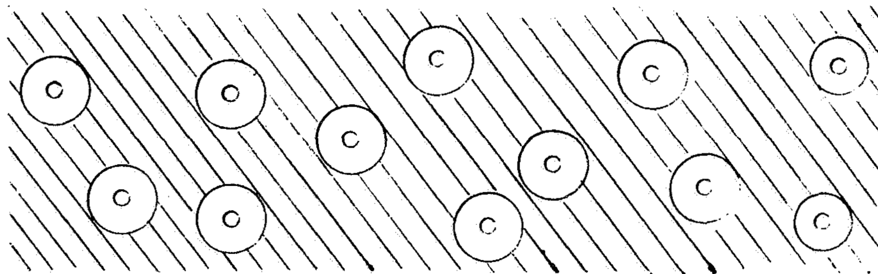

where the circular contours represent accumulation sites at two stages of oxidation. According to the present evidence the density of sites is about 1000/cm^2. The arrows indicate the directions of postulated oxygen ion surface migration. As oxide continues to accumulate the areas should grow larger, eventually comingling and producing a set of interstices at the same number density, pictured somewhat as follows:

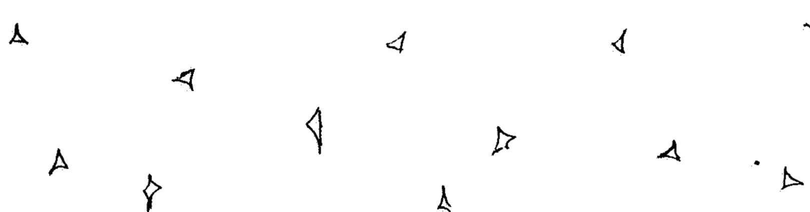

The interstices are in turn "filled in" at a random frequency, as evidenced by their exponential decay with oxide growth, producing the thin spots which later yield, in varying degrees, to such forces as compressive stress on cooling, electrophoretic decoration probing and shorting through the oxide on completed devices.

The model appears to explain the observations described above but is not proved by them. Nitric acid pretreatment introduces an oxide layer of something less than 250Å, as noted earlier. This layer may act to restrict lateral diffusion of oxygen ions at growth temperature, or it may contain an initial population of SiO_x which is more dense or continuous than SiO_x sites produced thermally, leaving a smaller number of oxide gaps to be filled in by conventional oxidation. On the other hand, slow growth of the first 250Å at 1180C would merely assure the discreteness of SiO_2 build-up around initial SiO_x sites. That is to say, it would do nothing to reduce the virtual defect density, as apparently observed.

Experiments planned for testing the model include the following: 1. Growth of 250Å oxide at high temperature according to the last described pretreatment, but without further subsequent oxidation, followed by tests for inhomogeneous distribution; 2. Exposure of nitric acid pretreated wafers to oxidation temperature in an inert ambient followed by tests to determine whether a nonhomogeneous distribution has been produced by the postulated lateral migration; 3. Prolonged pretreatment of wafers in hot nitric acid prior to oxidation to determine whether deeper layers provide better barriers to surface ion migration, or more uniform SiO_x distribution, as evidenced by the resulting virtual defect densities. If the proposed mechanism is borne out by these tests, a logical route to the elimination of dielectric defects will become possible.

2. Failure Mechanisms Associated with Packaging

Present process control of packaging techniques is inadequate in several respects and fosters a variety of modes of failure. These include variations in gas ambient compositions, nonhermeticity, corrosion of leads,

inferior heat sinks and cracked dice. These problems often are interdependent and augment each other or additional failure modes. Nonhermeticity may contribute to variations in package ambients and corrosion of leads; inferior heat sinks may contribute to cracked dice, degradation of h_{FE} and metallization mass transport, all of which are current reliability problems. Associated with the problem of nonhermetic packages is the lack of an adequate gross leak test. The objective of this investigation is to locate the sources of these problems in process control techniques and to seek remedies therefor.

Previous program activities in this area have been limited mainly to the analysis of package ambients and the investigation of the effects of certain of these gases on transistor function. Using mass spectrometric and gas chromatographic techniques a large variety of gaseous species were detected in the packages of transistors and integrated circuits. It was shown that the presence of moisture seriously affected the low temperature performance of mesa transistors but not of planar transistors. It also was shown that baking for limited periods in a hydrogen ambient produced irreversible increases in the betas of some groups of transistors but not in others. General conclusions could not be reached because of the limited sampling and the insufficiency of available process histories.

The rather surprising variety of gas compositions detected in the packages of generally well-made components led to considerable concern regarding the possible effects of such gases on the long-term constancy of electrical parameters. Since it was not considered feasible to investigate the effects of all of these compositions experimentally an attempt was made to catalog potential interactions on the basis of available thermodynamic and kinetic data with the expectation that attention would be focused on strongly favored interactions and diverted from those that were unlikely or forbidden. This compilation is included in the present report as Appendix B. In its present form the report is somewhat oversimplified and neglects certain questions of interest, such as the simultaneous effects chemical and electrical potentials or the effects of certain decomposition intermediates. It should be regarded, therefore,

somewhat as an initial draft which, through subsequent expansion, will evolve into a useful tool in calling attention to potential failure modes and, hopefully, providing an estimate of pertinent reaction kinetics.

Following the investigations on transistors facilities were established for similar investigations on integrated circuits providing considerable flexibility in the selection of test ambient compositions, temperatures and pressures. Investigations also were extended into other problem areas, such as the development of a satisfactory gross leak test. The general approach to these problems consisted of examining current practice for clues to the process origins of component defects followed by chemical and instrumental failure analysis by established procedures.

A number of environmental tests were conducted on groups of GPA integrated circuits (type 947) with the purpose of establishing what effects the presence of ambient hydrogen would have on the long term performance characteristics. Accelerated effects were first sought under the simultaneous application of electrical load and thermal stress. This proved highly destructive to the devices, even at only 150 C, because of localized thermal excursions. Surviving devices, however, were found to have undergone no significant change in characteristics due to the presence of hydrogen (forming gas) in these tests.

In subsequent tests electrical bias was eliminated in order to achieve higher ambient temperatures without catastrophic destruction. For example, a group of integrated circuits showed no change in room temperature electrical performance after baking at 525 C for nineteen hours under nitrogen. A sample of identical devices, however, displayed substantial degradation of outboard transistor betas as a result of baking in vacuum. The degradation was just noticeable at 300 C but pronounced at 350 C. Further experiments showed that the betas could be restored by baking in hydrogen, nitrogen or forming gas, and that the degradation and restoration apparently may be repeated indefinitely.

On the basis of these and earlier results it appears that the effects, if any, of hydrogen ambients on planar devices are curative rather than degradative and are not likely to occur at significant rates except at

well above use temperatures. It also appears that hydrogen is not unique in this respect and that improvement in betas after vacuum baking may be effected by other gases, such as nitrogen. The precise reason for the effects of vacuum baking are not known at this time but may be of further interest in view of the deep space nature of NASA missions and the uncertainty of achieving absolute package hermeticity. The search for unique effects of hydrogen on planar devices, however, has been discontinued.

3. Failure Analysis Service

The objective of this service is to examine state-of-the-art components periodically for inhomogeneities arising from process techniques. These analyses are being performed in detail on components important to the Failure Mechanisms Branch, Qualifications and Standards Laboratory, NASA-ERC. This effort constitutes a support function which is expected to reveal hitherto unsuspected inadequacies associated with fabrication steps as well as to characterize salient reliability problems peculiar to components from specific sources. Component anomalies are being examined by established failure mechanism techniques from which performance predictions can be derived appropriate to the long term reliability and environmental requirements applicable to NASA missions. Analytical results are independently summarized on each group of components. Groups are identified by Case Number, and individual specimens by Lot Number, Part Number and Sample Number. Clarification of test techniques and instrumentation, where required, is given in the Instrumental Capability Profile following this section. Analysis of Case Number CQF-101, consisting of 89 npn transistors has been completed.

4. Instrumental Capability Profile

The objective of this effort is to apprise NASA-ERC of optimum instrumentation and test sequences from which maximum insight into failure mechanisms may be gained. Original tabulations were presented in the second Monthly Report and Quarterly Report Number One, giving instrumental

capability ranges, applications to failure mode and failure mechanism investigation and references to pertinent process steps. Supplementary instrumental data have been presented in various succeeding reports. Continuing efforts in this area are intended to ensure the awareness of NASA-ERC of current instrumental innovations for extracting maximum failure information. On the following pages the most recent updating of this compilation is presented in tabular form.

Present information on the development of improved package leak tests is not sufficiently organized to be included in the accompanying tabulation and will be summarized at a later date. Two promising methods, however, are emerging, both of which are claimed to accommodate the combined ranges of gross and fine conventional tests. These are the sulfur hexafluoride test and the helium excitation transfer test.

In the sulfur hexafluoride test provision is made to inoculate the package under pressure without a previous outgassing. The inoculated package then is connected to a vacuum system containing a cold trap which condenses any SF_6 pumped out of the package. The condensate is thereby localized in a small volume from which it may be conveniently evaporated and admitted to a gas chromatograph for analysis. Recent results have shown the test to be operable from a lower leak rate of 5×10^{-7} std cc He/min up to that of a .013 inch diameter hole (#80 drill hole). Correlation with the standard helium leak rate test is uncertain at present mainly because of uncontrolled test variables in the conventional method. The sulfur hexafluoride method is tedious, a factor which may cancel out the elimination of two separate leak tests. However, in the upper range it is far more reliable than the present gross leak test.

The second technique depends on the transfer of excitation energy from a flowing stream of previously excited helium atoms to molecules of nitrogen or hydrogen escaping from the leak in the package. The leak is "detected" downstream from the package as a photoemission (fluorescence) as the excited molecules return to their ground state, or by measurement of the accompanying ionization effects. The helium is initially excited by an rf field or by beta emission from a tritium source. The test requires

INSTRUMENTS FOR FAILURE ANALYSIS

Instrument	Abnormality observed (physical)	Related failure modes	Probable failure mechanisms
Dye penetrant	Cracks in package seals	Leaks	Inversion (change in semi-conductor type)
Etching and microscopy	Dislocation distribution	Soft junction (gradual rather than sharp increase in current characteristic across junction)	Electrical parameter drifts
	Pits, cracks, and chips	Opens	Mechanical failure
	Pinholes and cracks in oxide insulating layer	Shorts	Migrating of metallization
Binocular micro-scope (3-120X magnification)	Inhomogeneity (Oxidation, contamination, intermetallics or rub marks.)	Weak bonds or electrical leakage	Poor surface wetting Migration of charged con-taminant causes inversion. Intermetallics form by diffusion. May have resulted from over-heating.
	Opened bonds	Electrical open circuit	Mishandling, overheating, or contaminated surface.
	Cracked dice	Open circuit or shift in resistance	Pressure during die or lead bonding.
	Cracks in package lead seals	Leaks	Rough handling, misalignment, thermal mismatch, or bubbles in glass.
	Pits and pyramids on dice	High leakage or hot spots at thinner base areas	Poor epitaxial growth control results in thin localized base areas (after diffusion).

C5-1471.11/3111

INSTRUMENTS FOR FAILURE ANALYSIS

Instrument	Abnormality observed (physical)	Related failure modes	Probable failure mechanisms
Binocular microscope (3-120X magnification) (cont'd)	Poor registry or masking	High leakage, shorts or opens	Narrow insulating path may short, or inversion may cause high leakage current.
	Scratches on dice or intraconnects	Open or high resistance	Handling and testing.
	Microplasma in operating device	Soft junction	Current concentrates at stacking faults, dislocations, or thin spots in base.
Phase contract microscope	Stacking faults	Soft junctions	Shifting electrical parameters.
	Transparent contaminants	Surface inversion	Ionic contaminants migrate and result in reverse leakage.
	Improper oxide metallization topography	Electrical leakage, shorts, or opens	Misalignment creates narrow insulating paths which short or leak as result of inversion.
Dark field microscope	Photoresist residues, dust	Inversion	Diffusion of charged contaminants.
	Bubbles in sealant glass	Leaks	Inversion.
Interferometer	Oxide and surface topography varies from design	Electrical leakage, shorts or opens	Misalignment creates narrow insulating paths which short or leak as result of inversion. Meager contacts melt and open.
	Oxide thickness varies from design	Stray capacitance, electrical leakage or inversion	Metal diffuses through oxide and causes leakage.
	Metal thickness varies from design	Opens	Thin metal areas burn out.

INSTRUMENTS FOR FAILURE ANALYSIS

Instrument	Abnormality observed (physical)	Related failure modes	Probable failure mechanisms
Electron microscope (magnifies to 100,000X)	Dislocation and stacking faults distribution	Soft junctions	Precipitates in bulk silicon.
	Contaminant and corrosion location	Weak bonds or electrical leakage	Electrochemical reaction.
	Etch pits, scratches, dust, and deposit roughness	Opens, shorts, or parameter drift	Surface roughnesses cause thin spots in conductor deposits which may heat and melt.
	Pattern alignment and topology errors	Shorts or opens	Meager contacts burn open. Narrow isolation areas short across.
	Undercut etched edges	Opens or inversion	Contaminants cause corrosion and opens or migrate and cause inversion.
	Weld porosity	Contaminants	Contaminants cause corrosion and opens or migrate and cause inversion.
	Porous diffusion products	Contaminants or weak bonds	Contaminants cause corrosion and opens or migrate and cause inversion. Kirkendall effect (mismatched diffusion rates of dissimilar metals) causes voids. Thin spots may heat and melt.
	Scribe cracks	Opens (if cracks propagate)	Thermal or mechanical stress causes cracks to propagate.
Radiographic equipment	Voids in welds	Leaks in package; opens if voids are associated with bonding of wires and package to IC die	Inversion corrosion, poor welding control.

INSTRUMENTS FOR FAILURE ANALYSIS

Instrument	Abnormality observed (physical)	Related failure modes	Probable failure mechanisms
Radiographic equipment (cont'd)	Metal migration	Shorts or opens	Kirkendall voids form weak bonds.
	Contaminant particles	Shorts	Mobile metallic contaminants shorts.
	Cracks	Opens or leaks	Cracks propagate and open connections.
	Long wires	Shorts	Wires sag, cause shorts.
	Misalignment of metal parts	Leaks, opens, or shorts	Misalignment causes weak bonds, shorts, opens, or leaky packages.
Controlled etching	Depth of inversion charge	Inversion	Inversion
X-ray diffraction	Identity of contaminant compounds or corrosion product compounds	Weak bonds or electrical leakage	Electrochemical reaction
	Identity of materials	Abnormal electrical parameters	Drift of electrical parameters.
Metallograph	Observes same abnormalities as binocular microscope; also:		
	Poorly adherent interconnects or bond structures	Opens	Improper deposition and/or bonding conditions.
	Abnormal junction depth (by angle lapping)	Improper electrical characteristics.	Bad junction depth.
	Voids in thermo-compression bonds	Bond has high electrical and/or thermal resistance and may be mechanically weak	Hot spots, poor electrical characteristics or opens.

INSTRUMENTS FOR FAILURE ANALYSIS

Instrument	Abnormality observed (physical)	Related failure modes	Probable failure mechanisms
Metallograph (cont'd)	Incomplete or poor welds	Leak in package	Faulty package seals.
	Thin or nonadherent plating	Poor joints	Opens bonds and/or package leaks.
Electron back-scatter thickness meter	Thickness of oxide, plating or photoresist	Stray capacitance, electrical leakage, inversion or opens	Electrical parameter drift

Instrument	Abnormality observed (chemical)	Related failure modes	Probable failure mechanisms
Hot stage metallograph	Contaminant melting point and reactivity (for identification)	Weak bonds or electrical leakage	Electrochemical reaction.
	Interdiffusion of metals, for example, Al-Au, Mo-Au, Ti-Au, Kovar-Au	Parameter drift	Intermetallics form from diffusion.
	Whisker growth	Shorts or opens	Metal whiskers grow and make shorts. Removal of metal leaves opens.
	Grain growth	Parameter drift	Drift in braze, bond, or interconnect resistance.
	Surface diffusion of metal films	Shorts, opens or parameter drift	Metal films cause shorts or inversion. Lack of diffusion barriers.
Electron diffraction	Contaminant crystal structure and identity of intermetallic compounds	Weak bonds or electrical leakage	Electrochemical reaction.
	Deposit crystallinity	Open, shorts, or parameter drift	

INSTRUMENTS FOR FAILURE ANALYSIS

Instrument	Abnormality observed (chemical)	Related failure modes	Probable failure mechanisms
Low-energy electron diffraction	Presence of absorbed substances in surface	Inversion	Migration of charged absorbates causes inversion.
Electron micro-probe (elemental chemical analysis)	Contaminant or rub mark residue identity and map	Weak bonds or electrical leakage	Migration of charged contaminants causes inversion.
	Dopant and dopant concentration	Related to process control	
	Intermetallic analysis	Weak bonds or electrical leakage	
	Corrosion product identity	Weak bonds or electrical leakage	
	Deposit topography map by chemical element	Opens, shorts, or parameter drift	
	Deposit thickness map by chemical element	Opens	Thin areas melt and open.
	Crack, pit, and pinhole maps	Opens or shorts	Thin or narrow areas on interconnects open. Pinholes.
	Junction misalignment or movement	Electrical leakage, shorts, opens, or inversion	Migration of metal is evidence of inversion.
	Opens, short and current and/or voltage nonuniformity map	Abnormal electrical parameters	Cause of abnormal electrical parameter may pinpoint failure mechanism.
Gas chromatograph	Abnormal package ambients	Inversion or grain drift	Absorption, then charge migration causes inversion.
	Leaks (by presence of air or test fluid)	Inversion or grain drift	Absorption, then charge migration causes inversion.
Mass spectrograph	Leaks. Also: reaction of device to ambient changes in the spectrograph	Inversion or grain drift	Absorption, then charge migration causes inversion.

C5-1471.11/3111

INSTRUMENTS FOR FAILURE ANALYSIS

Instrument	Abnormality observed (chemical)	Related failure modes	Probable failure mechanisms
Gas chromatograph and mass spectrograph in combination	Leaks. Also: reaction of device to ambient changes in the spectrograph	Inversion or grain drift	Absorption, then charge migration causes inversion.
Infrared absorption spectrograph	Thin oxide	Shorts or electrical leakage	Abnormal electrical parameters.
	Abnormal oxygen content in silicon	Drift of electrical parameters	Recombination centers.
	Abnormal epitaxy thickness	Slow switching, punch-through	Drift of marginal electrical parameters.
	Impure photoresist	Inversion	Migration of impurities.
	Water	Surface current leakage	Water vapor enters through leak.
Emission ultraviolet and visible spectrographs	Analysis and identity of contaminants	Parameter drift, opens, inversion	Contaminants migrate and change electrical properties or cause corrosion.
Visible and ultraviolet absorption spectrographs	Analysis and identity of contaminants	Parameter drift, opens, inversion	Contaminants migrate and change electrical properties or cause corrosion.
Neutron activation analyzer	Same as emission spectrograph but at lower concentrations	Parameter drift, opens, inversion	Contaminants migrate and change electrical properties or cause corrosion.

INSTRUMENTS FOR FAILURE ANALYSIS

Instrument	Abnormality observed (mechanical)	Related failure modes	Probable failure mechanisms
Strain gauges	Loose headers or dice	Thermal	Nonadhesion of braze evident from thermal expansion of can. Poor thermal path causes overheating.
	Poorly brazed headers or dice	Thermal	Nonadhesion of braze evident from thermal expansion of can. Poor thermal path causes overheating.
Bubble tester	Gross leaks in packages	Channeling or inversion	Nonadhesion of braze evident from thermal expansion of can. Poor thermal path causes overheating.
		Opens or shorts	Corrosion causes opens or shorts.
Helium leak tester or Radioflo tester	Small leaks	Uncontrolled package ambient causes inversion and corrosion	Charged adsorbates from ambient migrate and cause inversion. Corrosion by ambient causes opens or shorts.
Thermal plotter	Hot spots due to voids	Excess currents	Material degradation.
	Hot spots due to thin base areas	Excess currents	Uneven diffusion and thin base areas.
	Hot spots due to dislocation or stacking faults	Excess currents	Faster diffusion along fault causes thin base area.

C5-1471.11/3111

INSTRUMENTS FOR FAILURE ANALYSIS

Instrument	Abnormality observed (electrical)	Related failure modes	Probable failure mechanisms
Curve tracer	Shorts	Shorts	Sagging wire, punch through or surface creep of metal.
	Opens or intermittent contacts	Opens or intermittent contact	Mishandling, intermetallic formation.
	Soft junctions	Soft junctions	Surface leakage.
	Abnormal resistance	Abnormal resistance	Mechanical damage or corrosion.
	Leakage currents and inversion	Inversion	Surface charge migration or surface contamination.

SENSITIVITIES OF INSTRUMENTS

(Physical Properties)

Instrument and Procedure	Parameters Measured	Sensitivity,* Resolution or Power
Optical microscope Phase contrast	Surface topography Stacking faults	3X to 2000X, 0.5 micron To 1000X, 0.5 micron
Electron microscope	Crystal imperfections Dislocations & stacking faults	10 angstroms, 300,000X 100 angstroms apart
Interferometer Single beam Multiple beam	Film thickness or surface roughness	 300 angstroms 25 to 10 angstroms
Proficorder	Surface texture	100 angstroms
Contour projector	Surface contour along a line shadow	10 microns
Ellipsometer	Film thickness, dielectric Film thickness, silicon	2 angstroms 10 microns
Electron diffractograph Reflection Transmission	 Crystal character Crystal lattice parameters	 0.01 angstroms
Low energy electron diffraction (400)	Surface structure (generally) indicates presence of adsorbed materials	1 to 2 atomic layers deep
Scanning electron microscope	Device topography, voltage contrast	0.05 to 0.5 micron, 50,000X
Radiography unit	Inner topography	0.1 micron
X-ray diffraction	Phase analysis Crystallite size Dislocation mapping	0.5% to 10% 0.05 to 0.3 and 10 to 1,000 micron ranges Over 5 microns apart 5,000 psi or 500 ppm strain over area 0.010 in. across
Strain gauges	Strain, thus stress	1 ppm over .015 in, 100 pico strains
Tensile testers	Bond strength	0.1 gram
Thermal plotter	Surface temperature	2°C over .35 mil, 0.5°C over 1 mil diameter
Etching	Dislocations or stacking faults	10 microns apart

SENSITIVITIES OF INSTRUMENTS

(Electrical Properties)

Instrument and Procedure	Parameters Measured	Sensitivity,* Resolution or Power
Oscilloscopes	Current and Voltage	10^{-9} amperes
Ammeters, electrometers	Current	10^{-17} amperes
Voltmeters, Potentiometer	Voltage difference	5×10^{-10} volts
Capacitance bridges	Capacitance	10^{-17} farads, static
Ohmmeter, bridge	Resistance, impedance	10^{-8} to 10^{14} ohms

(Chemical Properties)

Instrument and Procedure	Parameters Measured	Sensitivity, Resolution or Power
Absorption spectroscopy atomic	Detection of metallic & semi-metallic elements	65 elements in ppm.
Infrared, attenuated total reflection	Surface composition	Depth is about 1 wavelength, depending on the angle of reflection.
X-ray spectroscopy	Chemical composition, oxidation state	10 to 1,000 ppm
Emission spectroscopy	Chemical composition	
Visible		1 ppm of most elements
X-ray		10 ppm of most elements
Neutron activation	Concentration of impurities	1 ppb of most elements, 1 ppm of oxygen
Mass spectroscopy	Chemical composition	
Gas		0.02 to 200 ppm 10^{-13} torr
Spark		1 ppb of many elements 20 to 200 ppb of H, N, C, O
Sputter		1 to 10 ppm in surface which is removed at 10 to 100 monolayers per second. Area 0.1 mm across may be analyzed.
Gas chromatography	Chemical composition	1 ppb hydrocarbons on milligram sample 1 ppm H, 10 ppm Ar, 50 ppm water
Electron spin resonance	Dangling bonds, free radicals, excited states	10^{11} H electron spins per gauss with 1 second integration time.

SENSITIVITIES OF INSTRUMENTS

(Electrical Properties)

Instrument and Procedure	Parameters Measured	Sensitivity,* Resolution or Power
Nuclear magnetic resonance	Molecular structure	2,000 ppm, 3×10^{18} spins/cm^3
Charged particle spectroscopy	Surface contaminant identification	Atomic number difference of 1
Electron microprobe		
X-ray mode	Identification & amount of chemical elements	10 ppm in bulk (1,000 ppm for lightest elements)
Backscattered electrons	Relative At. No variations	0.5 to 1 micron
Specimen current mode	Device topography	
Wet chemistry	Chemical composition	
Colorimetric		10 picograms
Fluorimetric		1 picogram of most elements
Ion exchange		Concentrates ions 100X
Carbon analyzer	Carbon determination	10 ppm
Vacuum fusion	Chemical composition	50 ppb H, 200 ppb or O or N

*Sensitivities quoted are the highest given in apparatus maker's literature.

ultrapure helium but is simple and rapid, and the required instrumentation is relatively uncomplicated. At the present time it appears to exceed the range covered by the sulfur hexafluoride test. However, considerable work is still required to establish a quantitative correlation between instrumental readings and actual leak rates.

Further results on these and other techniques will be reported as they become available.

COMPLETION INFORMATION

Approximate physical completion (current fiscal year)	60%
Approximate expenditures	58%

ACTION REQUIRED BY NASA

None

ACKNOWLEDGEMENTS

Contributions to the work reported herein were made by A.G. Buyers, R.O. Fewell, T.E. Hagey, Jr., S.J. O'Donnell, C.W. Scott, and W.W. Weller.

REFERENCES

1. J.E. Meinhard, "Hydrogen Isotope Investigation of Passivation Silicon Oxides", delivered at the Electrochemical Society Meeting, Cleveland, Ohio, May 3, 1966.

2. P.J. Besser, J.E. Meinhard, and P.H. Eisenberg, "Factors Influencing Dielectric Defects in Silicon Oxide Layers", delivered at the Electrochemical Society Meeting, Philadelphia, Pennsylvania, October 13, 1966.

3. D.J. McAdam, G.W. Geil, J. Research Natl. Bur. Standards 28, 593 (1942).

4. J.T. Law, J. Phys. Chem. 61, 1200 (1957).

5. J.W. Evans, S.K. Chatterji, J. Phys. Chem. 62, 1064 (1958).

6. J.R. Lizanga, W.G. Spitzer, Phys. & Chem. Solids 14, 131 (1960).

7. P.J. Jorgenson, J. Chem. Phys. 37, 874 (1962).

8. B.E. Deal, J. Electrochem. Soc. 110, 527 (1963).

9. B.H. Clausen, M. Flower, ibid, p. 983.

10. Quarterly Report No. 10, November 15, 1967.

APPENDIX A

MEASUREMENT OF COMPRESSIVE STRESS IN OXIDE LAYERS

The compressive stresses associated with oxide layers of various thicknesses and defect densities are listed in Table A-I. Determinations were made by Proficorder tracing arranged to give both the step thickness of an etch mark and the delta curvature, or deflection, over a given trace distance produced by removal of an oxide layer. From the deflection data the compressive stress is computed using the following relation:

$$\theta_o = 4E_s Z_s^2 d_s / 3Z_o l^2 \qquad (2)$$

where E_s is the modulus of elasticity of silicon (27.3 X 10^{-6} psi), Z_s and Z_o are the thicknesses (inches) of the silicon and oxide layers respectively, d_s is the deflection produced by oxide removal and l is the length of Proficorder traverse, yielding the compressive stress, θ_o, in psi. Mutually perpendicular Proficorder traces were made on each wafer.

Error in these measurements arose from two sources: step thickness determinations (±250Å) and curvature irregularities in about 50 percent of the Proficorder traces. The thickness error is apparent from Table I where the calculated stresses deviate from the average most for the thinner oxides (i.e., where the measurement error is proportionately greater). There is, however, no apparent change in stress with oxide thickness, as as deduced earlier from more limited evidence. Curvature irregularities were dealt with by area summation technique applied to the regions enclosed by the pre- and post-oxide removal curve traces. This resulted in an improvement of about 50 percent (to ±6.4 percent) over earlier computations.

The magnitude of the compressive stress in the oxide (4 X 10^{-4} psi) is considered substantial enough to rupture a large proportion of existing thin spots in the oxide on cooling from the oxidation temperature. Other thin spots, although fractured, may be held together by the residual compressive stress and escape detection by electrophoretic decoration.

These spots appear in turn to be opened up (i.e., they become detectable by decoration) by the convex curvature and relief of stress introduced by back oxide removal. The convex curvature is of course, readily apparent from the Proficorder traces.

TABLE A-I. CORRELATION OF DEFECT DENSITIES WITH OXIDATION AND STRESS

	Oxidation		Defects vs Stress (No./wafer)			Measured
Run	time, $t^{\frac{1}{2}}$ (minutes)	thickness (Angstroms)	No Stress[a]	Full Stress[b]	Partial Stress[c]	Stress[d] (psi x 10^{-3})
A	2.24	1720	131	545	987	40.3
B	3.16	1995	35	511	644	49.5
C	3.87	2590	10	343	479	36.8
D	4.47	3125	5	111	146	40.0
E	5.00	2945	8	170	353	42.1
J	5.00	3760	0.5	205	333	37.3
F	6.32	4010	1	31	140	41.4
G	7.81	5325	0	24	90	42.6
					Av:	41.3 ±6.4%

a. Silicon etch pit count produced before cooling.

b. Decoration count after cooling.

c. Decoration count after removal of back oxide layer.

d. By Proficorder trace method described in text.

APPENDIX B

THERMODYNAMIC ANALYSIS OF AMBIENT GAS EFFECTS

Introduction

Silicon device and integrated circuit technology, which represents one of the major areas of progress in electronics, depends heavily on the sophisticated use of highly specialized materials. The juxtaposition of such materials needed to produce the desired electronic function also often contains the seeds of long-term drift or deterioration of that very function. The mechanistic reasons for this frequently are unobvious because of the specialized nature of the materials and the intricate manner in which they are assembled. As a first step in anticipating such long-term interactions it should at least be determined which of them are thermodynamically permissible and which can be eliminated from further consideration. The present analysis attempts to do this for gaseous components that have been encountered by instrumental techniques, such as gas chromatography and mass spectrometry, in the packages of integrated circuits.

Gases considered were: nitrogen, hydrogen, argon, helium, methane, oxygen, water vapor, carbon dioxide, carbon monoxide, benzene, toluene, methylcyclohexane, and freon. Additional gases will be included as they are revealed by instrumental analysis.

Solid surfaces under examination were: silicon, silicon dioxide, aluminum, and aluminum oxide. Other surface compositions will be added in order of frequency and general reactivity.

Chemical reactions for the foregoing gases and solids were considered in terms of the simple thermodynamic free energy of reaction.

A literature survey concerned with integrated circuits and ambient gases is appended.

Free Energy Values

An important thermodynamic property is the free energy of reaction, for it is the magnitude and algebraic sign of this quantity which describes the chemical species which will exist under equilibrium conditions at a given temperature. Thus, the free energy of reaction or the change in free energy for a chemical reaction and its sign offers a means for the prediction that ambient gases will or will not chemically react with the solid surface materials present in packaged integrated circuits. With this connotation in mind Tables B-I and B-II summarize pertinent standard free energy values for temperatures, 298, 500 and 1000°K. The standard state is 298°K at atmospheric pressure. For gases a correction must be made for fact that a real gas is not a perfect gas.[1] Furthermore, it is important to note that the standard free energy of formation of an element is, by definition, zero for the standard state. It is through application of equation (1) that the standard change in free energy is calculated for possible chemical reaction between ambient gases and solids in packaged integrated circuits.

TABLE B-I. THERMODYNAMIC VALUES FOR AMBIENT GASES[2][3]

Gaseous Species	Standard Free Energy of Formation Kcal/Mole and ev					
	298°K	500°K	1000°K	298°K	500°K	1000°K
	Kcal/Mole			ev		
N_2, H_2, A, He, O_2	0	0	0	0	0	0
CH_4	-12.1	-7.8	+4.6	-0.53	-0.34	+0.20
HCl	-23.0	-24.0	-25.0	-1.00	-1.04	-1.09
H_2O	-54.6	-52.0	-46.0	-2.38	-2.26	-2.00
CO	-32.8	-37.1	-47.9	-1.43	-1.61	-2.08
CO_2	-94.3	-94.4	-94.6	-4.10	-4.11	-4.12
Benzene, C_6H_6	+31.0	+39.2	+62.3	+1.35	+1.71	+2.72
Toluene, C_7H_8	+29.3	+41.8	+76.3	+1.27	+1.82	+3.54
Methylcyclohexane, C_7H_{14}	+6.5	+37.5	+119.0	+0.28	+1.63	+5.18
CCl_2F_2	-102.7	-96.4	-81.2	-4.46	-4.19	-3.53
SiO_2(g)	-76.5	-76.8	-76.9	-3.33	-3.34	-3.35
SiO(g)	-27.9	-30.1	-42.2	-1.21	-1.31	-1.83
SiH_4	+13.2	+17.3	+28.8	+0.58	+0.75	+1.25
AlC	+196.2	+186.9	+164.5	+8.54	+8.14	+7.17
AlH	+55.0	+50.6	+40.6	+2.39	+2.20	+1.77
$SiCl_4$	-132.0	-128.0	-108.0	-5.75	-5.56	-4.70
SiF_4	-360.0	-356.0	-340.0	-15.70	-15.50	-14.80

TABLE B-II. THERMODYNAMIC VALUES FOR AMBIENT SOLIDS(2)(3)(4)

Solid Species	Standard Free Energy of Formation Kcal/Mole and ev					
	298°K	500°K	1000°K	298°K	500°K	1000°K
	Kcal/Mole			ev		
SiO_2	-204.6	-186.0	-164.0	-8.99	-7.80	-7.12
Al_2O_3	-378.1	-362.9	-325.3	-16.49	-15.80	-14.16
Si_3N_4	-36.0	-56.0	-100.0	-1.57	-2.44	-4.35
AlN	-68.6	-63.5	-50.5	-2.99	-2.77	-2.20
SiC	-20.1	-19.7	-18.8	-0.88	-0.86	-0.82
$AlCl_3$	-150.7	-138.8	-110.3	-6.55	-6.04	-4.80
AlF_3	-337.4	-324.6	-293.9	-14.69	-14.11	-12.75

Conclusions

The results of free energy calculations are summarized in Table B-III. The data predict for the indicated ambient gas-solid surfaces in contact, at the indicated temperatures, chemical reactions in all cases where the standard free energies are negative. These are the reactions between solid silicon and oxygen gas, solid silicon and carbon monoxide or carbon dioxide, gaseous benzene and solid silicon to form silicon carbide and hydride, toluene vapors and solid silicon to form the carbide or hydride, and CF_2Cl_2 and silicon to form silicon fluoride, silicon chloride and carbon.

Silicon dioxide solid is very stable and much less reactive than silicon. Free energy calculations for solid silicon dioxide with ambient gases were negative in only one instance, i.e., the chemical reaction with difluoro-dichloro-methane.

Aluminum metal is a common component in integrated circuit technology. Accordingly, simple standard free energies of reaction were calculated for solid aluminum-ambient gas systems. These thermodynamic data disclosed that the formation of aluminum nitride solid, aluminum oxide solid, (from both water vapor and oxygen, as well as carbon monoxide and dioxide), are probable reactions which occur between ambient gases and solids in packaged integrated circuits. As in the case of silicon metal and silica, the freon, dichloro-difluoro-methane, reacts with aluminum to form halide salts and carbon.

Aluminum oxide, solid, showed no chemical reactivity with any of the ambient gases commonly found in circuit packages.

A few general statements can be made concerning the calculated data in Table B-III.

(1) Only chemical reactions between ambient gases and solids most commonly used in packaged integrated circuits were considered. Other materials can be included.

(2) Free energy calculations for methylcyclohexane reactions are not shown as the results show that these reactions are less favorable than those of benzene and toluene.

TABLE B-III. CHEMICAL REACTIONS FOR PROCESS INTRODUCED AMBIENT GASES AT GAS-SOLID INTERFACES IN PACKAGED INTEGRATED CIRCUITS

	Reaction, Solid Silicon Ambient Gas	Free Energy of Reaction 298°K	500°K	1000°K	Favored
		Kca /Mole			
(1)	$Si_{(s)}+2H_{2(g)} \rightleftarrows SiH_{4(g)}$	+ 13.2	+ 17.3	+ 28.8	no
(2)	$Si_{(s)}+O_{2(g)} \rightleftarrows SiO_{2(s)}$	-204.6	-186.5	-164.0	Strongly
(3)	$2Si_{(s)}+O_{2(g)} \rightleftarrows 2SiO_{(g)}$	- 27.9	- 30.1	- 42.2	Yes
(4)	$Si_{(s)}+CH_{4(g)} \rightleftarrows SiH_{4(g)}+C_{(s)}$	+ 25.3	+ 25.1	+ 8.6	No
(5)	$Si_{(s)}+H_2O_{(g)} \rightleftarrows SiO_{(g)}+H_{2(g)}$	+ 26.7	+ 21.6	+ 3.8	No
(6)	$Si_{(s)}+SiO_{2(s)} \rightleftarrows 2SiO_{(g)}$	+148.8	+115.8	+ 79.6	No
(7)	$Si_{(s)}+2CO_{(g)} \rightleftarrows SiO_{2(s)}+2C_{(g)}$	-139.0	-111.8	- 63.2	Yes
(8)	$Si_{(g)}+2CO_{(g)} \rightleftarrows 2SiC_{(s)}+O_{2(g)}$	+ 25.4	+ 34.8	+ 58.2	No
(9)	$Si_{(s)}+CO_{2(g)} \rightleftarrows SiO_{2(g)}+C_{(s)}$	-110.3	- 91.6	- 69.5	Yes
(10)	$2Si_{(s)}+2CO_{2(g)} \rightleftarrows 2SiC_{(s)}+2O_{2(g)}$	+148.4	+149.4	+151.6	No

-3471.11/3111

TABLE B-III (Cont'd)

No.	Reaction, Solid Silicon Ambient Gas	Free Energy of Reaction 298°K (Kcal/Mole)	500°K (Kcal/Mole)	1000°K (Kcal/Mole)	Favored
(11)	$6Si_{(s)}+C_6H_{6(g)} \rightleftarrows 6SiC_{(s)}+3H_{2(g)}$	-151.6	-157.4	-177.1	Yes
(12)	$Si_{(s)}+C_6H_{6(g)} \rightleftarrows SiH_{4(g)}+6C_{(s)}+H_{2(g)}$	- 17.8	- 21.9	- 33.5	Yes
(13)	$7Si_{(s)}+C_7H_{8(g)} \rightleftarrows 7SiC_{(s)}+4H_{2(g)}$	-170.0	-179.7	-207.9	Strongly
(14)	$Si_{(s)}+C_7H_{8(g)} \rightleftarrows SiH_{4(g)}+7C_{(s)}+2H_{2(g)}$	- 16.1	- 24.5	- 47.5	Yes
(15)	$2Si_{(s)}+2CCl_2F_{2(g)} \rightleftarrows SiCl_{4(s)}+SiF_{4(s)}+2C_{(s)}$	-286.6	-291.2	-285.6	Strongly
(16)	$3Si_{(s)}+2N_{2(g)} \rightleftarrows Si_3N_{4(s)}$	- 82.0	-104.0	-150.0	Yes
(17)	$SiO_{2(s)}+2H_{2(g)} \rightleftarrows SiH_{4(g)}+O_{2(g)}$	+217.8	+203.3	+192.8	No
(18)	$SiO_{2(g)}+CH_{4(g)} \rightleftarrows SiH_{4(g)}+CO_{2(g)}$	+229.9	+211.1	+188.2	No
(19)	$SiO_{2(s)}+2H_2O_{(g)} \rightleftarrows SiH_{4(g)}+2O_{2(g)}$	+327.0	+301.3	+285.0	No
(20)	$2SiO_{2(s)}+2CO_{(g)} \rightleftarrows 2SiC_{(g)}+3O_{2(g)}$	+434.6	+406.8	+386.6	No
(21)	$SiO_{2(s)}+CO_{2(g)} \rightleftarrows SiC_{(s)}+2O_{2(g)}$	+278.8	+260.7	+240.0	No
(22)	$6SiO_{2(s)}+C_6H_{6(g)} \rightleftarrows 6SiC_{(s)}+3H_2O_{(g)}+9O_{2(g)}$	+880.9	+802.6	+670.9	No
(23)	$7SiO_{2(s)}+C_7H_{8(g)} \rightleftarrows 7SiC_{(s)}+4H_2O_{(g)}+5O_{2(g)}$	+1044.4	+914.3	+760.2	No

TABLE B-III (Cont'd)

	Reaction, Solid Silicon Ambient Gas	Free Energy of Reaction 298°K	500°K	1000°K	Favored
		Kcal/Mole			
(24)	$2SiO_{2(g)}+2CCl_2F_{2(g)} \rightleftarrows SiCl_{4(s)}+SiF_{4(g)}+2CO_{2(g)}$	- 66.0	-104.0	-131.8	Yes
(25)	$3SiO_{2(s)}+2N_{2(g)} \rightleftarrows Si_3N_{4(s)}+3O_{2(g)}$	+577.8	+502.0	+392.0	No
	Solid Aluminum-Ambient Gas				
(26)	$Al_{(s)}+\frac{1}{2}N_{2(g)} \rightleftarrows AlN_{(s)}$	- 68.6	- 63.5	- 50.6	Yes
(27)	$Al_{(s)}+\frac{1}{2}H_{2(g)} \rightleftarrows AlH_{(g)}$	+ 55.0	+ 50.6	+ 40.6	No
(28)	$2Al_{(s)}+3/2O_{2(g)} \rightleftarrows Al_2O_{3(s)}$	-378.1	-362.9	-325.3	Strongly
(29)	$Al_{(s)}+CH_{4(g)} \rightleftarrows AlC_{(g)}+2H_{2(g)}$	+208.3	+194.7	+159.9	No
(30)	$4Al_{(s)}+CH_{4(g)} \rightleftarrows 4AlH_{(g)}+C_{(s)}$	+232.1	+210.2	+157.8	No
(31)	$2Al_{(s)}+3H_2O_{(g)} \rightleftarrows Al_2O_{3(s)}+3H_{2(g)}$	-214.3	-206.9	-187.3	Yes
(32)	$2Al_{(s)}+3CO_{(g)} \rightleftarrows Al_2O_{3(g)}+3C_{(s)}$	-279.7	-251.6	-181.6	Yes
(33)	$6Al_{(s)}+C_6H_6 \rightleftarrows 6AlC_{(g)}+3H_{2(g)}$	+1146.2	+1082.3	+924.7	No
(34)	$4Al_{(s)}+3CO_{2(g)} \rightleftarrows 2Al_2O_{3(g)}+3C_{(s)}$	-473.3	-442.6	-366.8	Strongly
(35)	$8Al_{(s)}+C_7H_{8(g)} \rightleftarrows 8AlH_{(g)}+7C_{(s)}$	+410.7	+363.0	+248.5	No
(36)	$4Al_{(s)}+3CCl_2F_{2(g)} \rightleftarrows 3C_{(s)}+2AlCl_{3(s)}+2AlF_{3(s)}$	-668.1	-637.6	-564.8	Strongly

TABLE B-III (Cont'd)

	Solid Aluminum-Ambient Gas			Free Energy of Reaction 298°K	500°K Kcal/Mole	1000°K	Favored
(37)	$Al_2O_{3(s)}+N_{2(g)}$	$\rightleftarrows$	$2AlN_{(s)}+3/2O_{2(g)}$	+240.9	+235.9	+224.1	No
(38)	$Al_2O_{3(g)}+H_{2(g)}$	$\rightleftarrows$	$2AlH_{(g)}+3/2O_{2(g)}$	+488.1	+464.1	+406.5	No
(39)	$Al_2O_{3(s)}+2CH_{4(g)}$	$\rightleftarrows$	$2AlC_{(g)}+3H_2O_{(g)}+H_{2(g)}$	+625.9	+596.3	+501.1	No
(40)	$Al_2O_{3(s)}+H_2O_{(g)}$	$\rightleftarrows$	$2AlH_{(g)}+2O_{2(g)}$	+542.7	+528.1	+452.5	No
(41)	$\frac{1}{2}Al_2O_{3(s)}+CO_{(g)}$	$\rightleftarrows$	$AlC_{(g)}+5/2O_{2(g)}$	+418.0	+407.9	+375.1	No
(42)	$3Al_2O_{3(s)}+C_6H_{6(g)}$	$\rightleftarrows$	$6AlC_{(g)}+3H_2O_{(g)}+3O_{2(g)}$	+2116.7	+2013.9	+1766.6	No
(43)	$2Al_2O_{3(s)}+C_7H_{8(g)}$	$\rightleftarrows$	$4AlC_{(g)}+3CO_{(g)}+3H_2O_{(g)}+H_{2(g)}$	+1237.5	+1174.5	+628.0	No
(44)	$7Al_2O_{3(s)}+6CO_2F_{2(g)}$	$\rightleftarrows$	$6AlC_{(g)}+4AlCl_{3(g)}+4AlF_{3(g)}+21O_{2(g)}$	+1253.9	+1164.4	+1067.3	No
(45)	$2Al_2O_{3(s)}+3Si_{(s)}$	$\rightleftarrows$	$4Al_{(s)}+3SiO_{2(s)}$	+142.4	+168.8	+156.6	No

(3) No limits of error were associated with thermodynamic values used as they were not available in many cases.

(4) The predictions made concerning ambient gas-solid chemical reactions are for the equilibrium condition. The kinetic picture can be quite different. For example, the kinetic removal of one chemical product from the reaction at equilibrium can cause a complete shift in the equilibrium to form more of the reaction products. During this shifting condition the processes may be steady state and are kinetic in nature until the new equilibrium is achieved.

(5) Only over-all chemical reactions were considered. The participation of potential chemical intermediates and/or activated states was omitted from consideration.

(6) Reaction of hydrogen with Si, SiO_2, Al and Al_2O_3 is thermodynamically disallowed.

REFERENCES

1. G.N. Lewis and M. Randall, Thermodynamics, 2nd Edition, McGraw-Hill, New York, 1961.

2. Stull, D.R., Proj. Director, Janaf Thermochemical Tables, Advanced Research Projects Agency Program. US Air Force Contract No. AF04(611)7554 Dow Chemical Co., Midland, Michigan.

3. Glasser, A., "A Survey of the Free Energies of Formation of the Fluorides, Chlorides and Oxides of the Elements to 2500°K", ANL-5107, August 1953.

4. Chu, T.L., Lee, C.H., and Gruber, G.A., J. Electrochem. Soc., Solid State. 114, No. 7, 717-722 (1967).

BIBLIOGRAPHY (1925 - 1968)

1. Swets, D.E., Lee, R.W., Frank, R.C. "Diffusion Coefficient of Helium in Fused Quartz", J. Chem. Phys., 34, 17 (1961).

Diffusion coefficient of helium in silicon dioxide glass measured by permeation method using a mass spectrometer.

2. Leiby, C.C. and Chen, C.L., "Diffusion Coefficients, Solubilities and Permeabilities for He, Ne, H_2 and N_2 in Vycor Glass". J. Appl. Phys., 31, 268 (1960).

In 96% silicon dioxide glass (vycor) helium diffusion rate is higher than in pure silicon dioxide glass, but is lower in most other glasses. The higher diffusion rate in vycor is probably due to the method of fabrication leading to greater porosity.

3. Mouison, A.J., Roberts, J.P., "Water in Silica Glass", Trans. Brit. Ceram. Soc., 59, 388-399 (1960), Trans. Faraday Soc., 59, 1208-1216 (1961).

Diffusion measured by IR absorption at 2.7 microns. Some question as to whether water or hydroxyl is diffusing species.

4. Zaininger, K.H., Warfield, G., "Hydrogen Induced Surface States at a Si-SiO_2 Interface", Proc. IEEE, 52, 972-973, August (1964).

Hydrogen increases the inversion layer capacitance upon contact with an MOS structure at high temperature.

5. Haas, C. "The Diffusion of Oxygen Into Silicon," J. Phys. Chem. Solids 15, 108-111, August (1960).

Assumption is made that internal friction and diffusion, or both, due to the same relaxation phenomenon. The diffusion coefficient for oxygen in silicon is calculated from experimental data on internal friction. Diffusion constant: 0.21 cm^2/sec, energy of activation: 2.44 electron volts.

6. Logan, R.A. and Peter, A.J., "Diffusion of Oxygen in Silicon". J. Appl. Phys. 28, 819-820, July 19 (1957).

Experimental results on oxygen diffusion coefficient in silicon support Haas.

7. Frosch, C.J. and Derick, L. "Diffusion Control in Silicon by Carrier Gas Composition". J. Electro-Chem. Soc. 105, 695-699, December (1958).

Antimony tetroxide at 950°C, one hour diffusion at 1200°C produces a junction 1.5 microns deep in a 5 ohm-cm p-type

silicon. The surface concentration depends upon the quantity of water vapor in the nitrogen flow gas, from 3.3 X 10^{19} atoms/cm^{-3} for dry nitrogen to 8 X 10^{17} atoms/cm^{-3} for nitrogen bubbled through water at 70°C.

8. Thompson, C. "The Effects of Ambients on Performance of CdS Thin Film Transistors". Science Abstracts B. Electrical Engineering 68, 11389 (1965); Japan J. Appl. Phys. 4, No. 3, 207-211 March (1965).

   Describes the operating mechanisms of the thin film CdS transistor at several pertinent temperatures and ambients. The effects of the ambients are correlated to device parameters with further implications.

9. Lehman, H.S., "Chemical and Ambient Effects on Surface Conduction in Passivated Silicon Semiconductors". Science Abstracts B. Electrical Engineering 68, 9843 (1965); IBM J. Res. and Development (USA) 8, No. 4, 422-426 September (1964).

   The effect of processing variables on the surface conduction properties of passivated silicon junction devices has been studied. Insulated gate field effect transistors fabricated in p-type silicon were used as an experimental tool. Varying the metal used as the gate electrode is shown to strongly influence the surface conductivity of the field effect device. The effects of heat treatment in various ambients and variation in the insulators used are also discussed. Surface conduction is shown to be a complex function of materials thermal history and processing.

10. Brattain, V.H. and Garrett, C.G. "Protection of Silicon Conductive Devices by Gaseous Ambients". (Bell Telephone Lab.) US Pat. No. 2,777,974, January 15, 1957.

    The use of an ambient atmosphere of oxygen to control the surface characteristics of junction devices by preventing or inhibiting the formation of undesirable conducting paths (channels) at or near the surfaces of these devices is dis-discussed. The effects of the oxygen is to form a layer of p-type material on the surface of the crystal which prevents the formation of n-type channels on the p-type region.

11. Many, A. and Gerlick, D. "The Effect of Gaseous Ambients on the Interface Structure of Germanium. (Hebrew Univ.) Recent news abstracts of the Electrochem. Soc., Semiconductor Symposium, May (1957).

    Simultaneous measurements of surface recombination velocity and trapped charge density in the fast state as a function of surface potential were reported. The surface potential was varied over a wide range by the application of large AC fields normal to the surface. It was found that the distribution and characteristics of the fast state were markedly affected by the surrounding ambients. Initially with the sample in vacuum,

rapid changes in interface structure took place. After a few days stabilization was essentially reached. Following repeated exposures to the different ambients reproducible changes resulted which presisted for many weeks.

12. Jauffe, K. "Gas Reaction on Semiconducting Surfaces and Space Charge Boundary Layers". Semiconductor Surface Physics, Univ. of Pennsylvania Press, 259-282 (1957).

    The Fermi potential of a catalyst is related to the electronic exchange level of the reacting molecules. Applying a three dimensional term scheme the relations are generalized. On the basis of results one can determine whether an n- or p-type catalyst must be used for a reaction. Furthermore, the important rule of the space charge in the catalyst is discussed with its effect upon the reaction kinetics.

13. Stattz, H., DeMars, G.A., Davis, L. Jr., Adams, A. Jr., (Raytheon Manufacturing Co.) Semiconductor Surface Physics (University of Pennsylvania Press) 139-168 (1957).

    Steady state and nonsteady state inversion layer conductance on silicon and germanium are discussed in terms of two types of surface states. The second type state is located at the surface of the oxide with perhaps some states in the oxide film. The states result mainly from adsorbed gas molecules. Depending upon the surrounding gas they are either predominantly acceptor or donor type and it is principally the states which determine the directions in which the bands at the surface are bent. It is possible to determine the number and energy of the interface states from nonsteady state inversion layer conductance measurement. It is found that high fields across the oxide film can influence the density of these states in silicon lying above the middle of the gap. Anomalous inversion layer conductances are found when vapors of certain liquids are adsorbed.

14. Kozlouskaya, V.M. "Mass Spectrometric Determination of the Amount and Composition of Gases Adsorbed on the Surface of Germanium and Silicon Monocrystals". Solid State Abstract 1,6046 (1960-1961); Soviet Phys., Solid State 1, 940-946 January (1960).

15. Gleason, F.R., Greiner, J.H. and Yetter, L.R. "Gas Absorption by Vacuum Evaporated Magnetic Films". Solid State Abstract 1, 6149 (1960-1961); (IBM) Vacuum 9, 301 November (1959).

    Mass spectrometric determination of the types and amounts of gases absorbed during the deposition of vacuum evaporated thin films were reported. Most of the gases came from the oil pump. The absorbed gas molecules per metal atom degassed was independent of film thickness, indicating that the gas is trapped in the film structure as well as on the surface.

16. Kammere, H.C., "Thermal Evaluation of High Density Electronic Packages". Solid State Abstract 3, 16912 (1962) Electron Design 9, 121-122 December (1961).

A monograph to determine the design limitation of microminiature packages exposed to thermal stress. Five basic parameters investigated were: total temperature between ambient environment and the center of the package, thermal conductivity of package material, cooling technique and size and configuration of maximum.

17. Kislev, A.U. and Lygin, V.I. "University of Moscow". Solid State Abstract 5, 28828 (1964); Surface Science 2, 236-244 (1964).

The shift of the absorption band of silica surface hydroxyl groups on adsorption of molecules of different electronic structures is in accordance with their heats of adsorption and ionization potentials. On the basis of vibrational theory the spectra of water and ammonia molecules adsorbed on silica and zeolites have been analyzed.

18. Boutin, H. and Prask, H. "Study of Water Vapor Absorption on Gamma Alumina and Silica by Slow Neutron Inelastic Scattering". Solid State Abstract 5, 28830 (1964); Surface Science 2, 261-266 (1964).

The energy spectrum of neutrons, inelastically scattered by hydrogenous groups adsorbed on the solid surface is able to provide information concerning the degree of mobility of those groups, the nature and strength of the binding with the adsorbent and the frequencies of rotational or vibrational motions ranging from 20 to 1,000 cm^{-1}. The principle of the technique is given and is applied to water adsorbed on silica and gamma alumina after the samples have been heated to a 150° under vacuum. Two types of water molecules exist on the surface: distorted molecules with hydroxyl groups hydrogen-bonded to oxygen atoms, and tetrahedral molecules similar to the liquid. Additional water layers on the surface become more water-like.

19. Volkenstein, F.F. and Karpenke, I.V. "Theory of Photoadsorptive Effect in Semiconductors". Solid State Abstract 5, 30709 (1964); STAR 2, 3457A December (1964) AD605733.

The sign of the photo-adsorptive effect in semiconductors depends on selection of the system, on the mode of experiment and the preparation of the sample for experiment. Report offers formulas for establishing basic criteria for determination of the photo-adsorption effect.

20. Farnsworth, H.E. and Campbell, B.D. (Brown University) "Study of the Surface Properties of Atomically Clean Metal and Semiconductors". Solid State Abstract 6, 37205 (1966); Contract DA28304 ANC 0029E US Government Research and Development Reports 40, 146A May 20, (1965) AD 31-699.

Oxygen adsorption on the (0001) matte surface was enhanced when an intense light was incident on the crystal. A 3-5 Torr-min oxygen exposure in intense light extinguished the diffraction pattern whereas a 759 Torr-min exposure in the dark had little effect upon the pattern, but did cause a slight decrease in conductivity of the surface. Ion bombardment increased the dark conductivity and greatly decreased the effect of intense light. Photo-adsorption of oxygen is indicated. Unlike matte surface (0001) specular surface was not effected by exposure to light.

21. Hobson, J.P. "A New Method for Finding Heterogeneous Energy Distributions from Physical Adsorption Isotherms". Solid State Abstracts 6, 41617 (1966); Canadian J. Phys. 4, 1934 November (1965).

    A model is described which assumes that a hetergeneous surface has a distribution of adsorption energies for physical adsorption. A new solution is presented giving a number of step types: local isotherms, which are chosen to represent varying degrees of adsorbate-adsorbate interaction. The solution permits energy distributions to be obtained quite simply from isotherm data at one temperature. This solution may be used to calculate isotherms at other temperatures.

22. Howling, D.H. "Photoelectric Response of Metal Surfaces in Ambient Atmospheres". Solid State Abstract 7, 48029 (1967); J. Appl. Phys. 37, 1844 (1966).

    Experiments are described which examine variations in the photoelectric response of metal surfaces immersed in gas atmospheres. Work function changes have been produced by gas bombardment, electrode heating, deposition of small amounts of K on the surface. By operating the electrode under study as the cathode of geiger muller photon counter, photocurrents as low as 10^{-21} A could be measured. Factors which influence irreversible changes in work functions have been explored. A less well known increase in work function which is thermally activated has been demonstrated. Systems included were: tungsten/hydrogen, nickel/hydrogen, iron/hydrogen, platinum/hydrogen, paladium/hydrogen, rhenium/hydrogen; also nitrogen, neon, argon and ammonia.

23. Logan, R.M. and Stickney, R.E., "Simple Classical Model for the Scattering of Gas Atoms from a Solid Surface". Solid State Abstract 7, 46668 (1967); J. Chem. Phys. 44, 195 (1966).

    A simple classical model for the scattering of gas atoms from a solid surface is proposed and its characteristics discussed. Results are obtained for the angular distribution of scattered particles. The model correctly predicts the general appearance of the scattering pattern, and its dependence upon the angle of incidence of the beam and on the temperature and masses of the gas and surface atoms.

24. Lu, Wei-Kao, "The General Rate Equation for Gas Solid Reaction in Metallurgical Processes with the Restrictions of Reversibility of Chemical Reaction and Gaseous Equimolar Counter-Diffusion". Solid State Abstract 7, 46669 (1967); AIME. Trans. 236, 531 (1965).

An improved general rate equation for a one dimensional gas-solid system has been derived. The concentrations of gaseous reactant and product have been calculated with relations furnished by the following constraints on the system: quasi-steady state and equimolar counter diffusion of gases. The interfacial chemical reaction is taken as 1st order with respect to the concentration of the gases involved. The equation has proper dependence on gas composition and on solid structure through the relative values of Knudsen and normal diffusivities.

25. Micheletti, F.B., and Mark, P., "Effects of Chemi-sorbed Oxygen on the Electrical Properties of Chemically Sprayed CdS Thin Films". Electronics and Communications Abstracts 6, 4467 (1967); Appl. Phys. Letters 10, No. 4, 136-138 (1967).

Measurements with spray deposited semiconducting CdS films are reported that demonstrate the primary effect of oxygen chemi-sorption is the reduction of hall mobility.

26. Blum, J., Warwick, R. and Genser, M. "Surface Studies with Silicon Planar Junction Structures". Presented at the Spring Meeting of the Electrochemical Society, Toronto, Canada, May 3-7 (1964) (Gen. Prec. Aerospace., Kearfott Div.)

Changes in: emitter current gain, beta, with collector current. Surface recombination velocity limits beta and is in turn determined by the density of fast interface states and the surface potential. Changes in characteristics of silicon npn planar transistors were observed after heating for various times at temperatures between 300-350°C in forming gas (15% H_2, 85% N_2), oxygen, vacuum and nitrogen.